

# CONTENTS

|  | Page |
|--|------|
| Acknowledgement  | c    |
| Abstract in Thai   | d    |
| Abstract in English                                      | f    |
| Contents   | h    |
| List of Tables   | k    |
| List of Figures  | l    |
| Chapter 1 Introduction                                   | 1    |
| 1.1 Problem Statement and Motivation                     | 1    |
| 1.2 Background of Study Area                             | 2    |
| 1.2.1 Basin Configuration                                | 3    |
| 1.2.2 Stratigraphy of the North Malay Basin              | 4    |
| 1.3 Objective  | 6    |
| 1.4 Literature Review                                    | 6    |
| 1.4.1 Rock Physics Inversion                             | 6    |
| 1.4.2 Pre-stack Inversion for Estimating Rock Properties | 7    |
| 1.5 Data Available                                       | 8    |
| 1.5.1 Well Log Data                                      | 8    |
| 1.5.2 Seismic Data                                       | 13   |
| 1.5.3 Interpretation Data                                | 14   |
| Chapter 2 Theories and Principles                        | 16   |
| 2.1 Rock Physics Modeling                                | 16   |
| 2.1.1 Gardner's relations                                | 16   |
| 2.1.2 Greenberg-Castagna                                 | 16   |
| 2.2 AVO Response and Classification                      | 17   |

|   |    |
|---|----|
| 2.2.1 AVO Intercept and Gradient                      | 18 |
| 2.2.2 AVO Classes                                     | 19 |
| 2.2.3 AVO Responses and AVO Crossplot                 | 20 |
| 2.3 Seismic Inversion                                 | 22 |
| 2.3.1 The General Assumptions for Seismic Inversion   | 22 |
| 2.3.2 Pre-stack Simultaneous Inversion                | 23 |
| Chapter 3 Methodology                                 | 16 |
| 3.1 Workflow  | 27 |
| 3.2 Rock Physic and AVO Modeling                      | 28 |
| 3.2.1 Well Log Conditioning                           | 28 |
| 3.2.2 Shear Wave Velocity Estimation                  | 31 |
| 3.2.3 Rock Physics Model                              | 33 |
| 3.2.4 AVO Modeling                                    | 39 |
| 3.3 Pre-stack Deterministic Inversion                 | 43 |
| 3.4 Lithology Delineation and Prospect Identification | 50 |
| Chapter 4 Results                                     | 51 |
| 4.1 Estimated Shear Wave Velocity                     | 51 |
| 4.2 Sonic Log Calibration and Well Correlation        | 52 |
| 4.2.1 Sonic Log and Checkshot Calibration             | 52 |
| 4.2.2 Seismic and Well Correlation                    | 52 |
| 4.3 AVO Responds                                      | 55 |
| 4.4 Initial Strata Model                              | 56 |
| 4.5 Inversion Analysis                                | 60 |
| 4.6 Pre-stack Seismic Inversion                       | 63 |
| 4.7 Lithology Delineation                             | 67 |
| Chapter 5 Discussion and Conclusion                   | 74 |
| 5.1 Discussion  | 74 |
| 5.2 Conclusion  | 78 |
| 5.3 Recommendation                                    | 78 |

|  |    |
|--|----|
| References   | 79 |
| Appendix   | 83 |
| A. Seismic Acquisition Parameters                        | 83 |
| A.1 Acquisition Program                                  | 83 |
| A.2 Energy Source Specifications                         | 83 |
| A.3 Seismic Recording and Streamer System Specifications | 84 |
| A.4 3D Binning and Binning Parameters                    | 84 |
| A.5 3D Acquisition Parameters                            | 85 |
| B. Seismic Data Processing Parameters                    | 85 |
| B.1 Summary of Pre-stack Time Migration Production       | 85 |
| B.2 3D Processing Flow Chart                             | 88 |
| Curriculum Vitae   | 89 |

ลิขสิทธิ์มหาวิทยาลัยเชียงใหม่  
Copyright© by Chiang Mai University  
All rights reserved

## LIST OF TABLES

|   | Page |
|---|------|
| Table 1-1 Relationship between interpreted horizons and geological markers  | 15   |
| Table 2-1 Examples of the five AVO classes assuming normal polarity   | 20   |
| Table 4-1 Minimum and maximum residual drift after sonic log calibration using polynomial fit to checkshot data   | 52   |
| Table 4-2 Bulk shift and correlation coefficient of each well   | 53   |
| Table 4-3 Summary of AVO classes and fluid of each sandstone reservoir  | 56   |
| Table 4-4 Summary of inversion parameters using for pre-stack seismic inversion   | 60   |
| Table 4-5 Error values between original well log and inverted well log together with correlation and error values of inverted synthetic comparing to seismic traces | 61   |

## LIST OF FIGURES

|             |  | Page |
|-------------|--|------|
| Figure 1-1  | Location of study area in North Malay Basin  | 2    |
| Figure 1-2  | The regional fault trends of the Tertiary basins in the Gulf of Thailand   | 3    |
| Figure 1-3  | Regional schematic stratigraphy of the North Malay Basin   | 5    |
| Figure 1-4  | Well tie of variable angle stacks  | 6    |
| Figure 1-5  | AVO inversion results and rock physics inversion results for well 2-21 of A Montney case study   | 7    |
| Figure 1-6  | Comparison of $V_P/V_S$ calculated from AVO + post-stack inversion, pre-stack inversion. $V_P/V_S$ from logs at Well D had been inserted in colour and the SP log as the trace | 8    |
| Figure 1-7  | Well logs and geological markers of R-2 well   | 9    |
| Figure 1-8  | Well logs and geological markers of D-36 Well  | 10   |
| Figure 1-9  | Well logs and geological markers of S-2 Well   | 11   |
| Figure 1-10 | Well logs and geological markers of G-29 Well  | 12   |
| Figure 1-11 | Well locations and seismic area which is filled by color bar of fold (maximum fold is 32) is 3D pre-stack seismic gathers combining to a 3D survey.                            | 13   |
| Figure 1-12 | Examples of pre-stack seismic data on Inline 1900 after NMO correction   | 14   |
| Figure 1-13 | Seismic section show interpreted horizons and faults in study area   | 15   |
| Figure 2-1  | P-wave velocity and density relationships in rocks of different lithology re-drawn after Gardner et al, 1974   | 17   |
| Figure 2-2  | Crossplot of Greenberg–Castagna $V_P$ – $V_S$ relations  | 17   |
| Figure 2-3  | Mode conversion of an incident P-wave on the boundary between two elastic layers in the subsurface of the earth  | 18   |

|             |  |    |
|-------------|--|----|
| Figure 2-4  | The AVO Classes modified after Rutherford and Williams, 1989, Ross and Kinman, 1995 and Castagna and Swan in 1997  | 19 |
| Figure 2-5  | The various AVO classes are described in different area on AVO crossplot   | 21 |
| Figure 2-6  | Schematic models for oil and brine sand response   | 21 |
| Figure 2-7  | The basic convolutional model of the seismic trace is Seismic Trace = Wavelet convolved with reflectivity plus noise   | 23 |
| Figure 2-8  | Crossplots of $\ln(Z_D)$ vs $\ln(Z_P)$ and $\ln(Z_S)$ vs $\ln(Z_P)$ where, in both cases, a best straight line fit has been added. The deviations away from this straight line, $\Delta L_D$ and $\Delta L_S$ , are the desired fluid anomalies. | 26 |
| Figure 2-9  | Matrix form of simultaneous inversion equation   | 26 |
| Figure 3-1  | Simplified workflow of methodology   | 27 |
| Figure 3-2  | Sonic log conditioning of S-2 Well after calibration with VSP using polynomial fit order 4 of created knees  | 29 |
| Figure 3-3  | Sonic log conditioning of R-2 Well after calibration with VSP using polynomial fit order 4 of created knees  | 29 |
| Figure 3-4  | Sonic log conditioning of D-36 Well after calibration with VSP using polynomial fit order 3 of created knees   | 30 |
| Figure 3-5  | Sonic log conditioning of G-29 Well after calibration with VSP using polynomial fit order 3 of created knees   | 30 |
| Figure 3-6  | The highlight zone of $V_P$ and $V_S$ that was used in $V_P$ - $V_S$ crossplot to find the best fit lines of sand and shale for estimating $V_S$ in D-36 well.   | 31 |
| Figure 3-7  | $V_S$ estimation showing log curves of GR, $V_P$ , original $V_S$ , combined $V_S$ , $V_S$ sand, $V_S$ shale, and final $V_S$  | 32 |
| Figure 3-8  | $V_P$ -Rho crossplot of four wells (S-2, R-2, D-36 and G-29)   | 33 |
| Figure 3-9  | $V_P$ -Rho crossplot of S-2 well   | 34 |
| Figure 3-10 | $V_P$ -Rho crossplot of R-2 well   | 34 |
| Figure 3-11 | $V_P$ -Rho crossplot of D-36 well  | 35 |

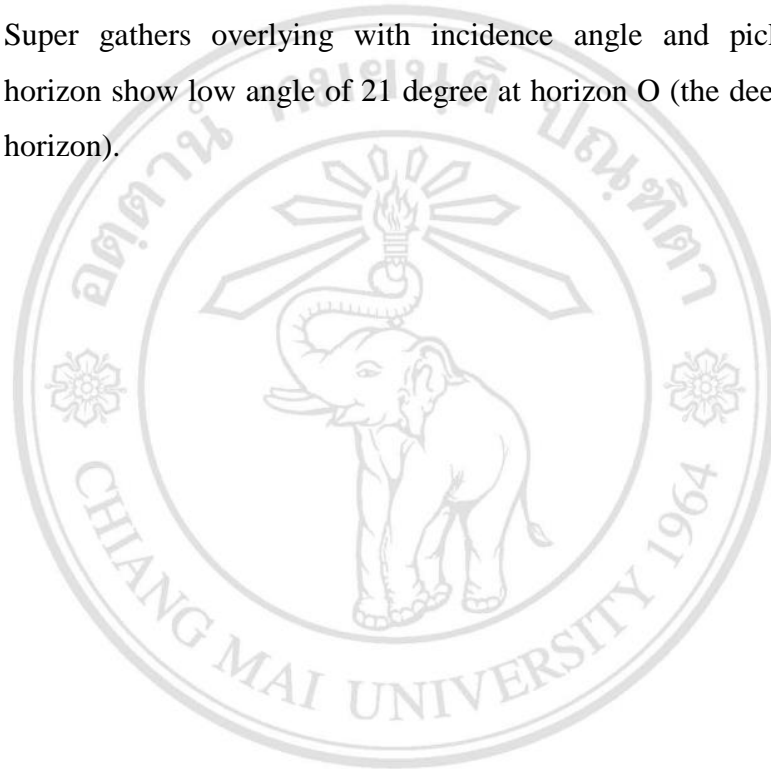
|             |  |    |
|-------------|--|----|
| Figure 3-12 | V <sub>p</sub> -Rho crossplot of G-29 well   | 35 |
| Figure 3-13 | V <sub>p</sub> -V <sub>s</sub> crossplot of D-36 well at Lower FM1 and FM0 where were acquired S-wave velocity are shown different shale and sandstone trends.                 | 36 |
| Figure 3-14 | V <sub>p</sub> -V <sub>s</sub> crossplot of R-2 well at Unit 2C to 2A and FM1 to FM0 showing different shale and sandstone trends.   | 37 |
| Figure 3-15 | V <sub>p</sub> -V <sub>s</sub> crossplot of S-2 well at Unit 2D to 2A and FM1 to TD showing different shale and sandstone trends.  | 38 |
| Figure 3-16 | AVO modeling of S-2 Well showing example intervals of water and gas, sandstone A shows AVO class IV, sandstone B, C and D show AVO class II.                                   | 39 |
| Figure 3-17 | AVO modeling of R-2 Well showing example intervals of water and gas, sandstone A shows AVO class IV, sandstone B, C and D show AVO class II.                                   | 40 |
| Figure 3-18 | AVO modeling of D-36 Well showing example intervals of water and gas, sandstone A, B and C show AVO class IV, sandstone D shows AVO class II, sandstone E shows AVO class IIp. | 41 |
| Figure 3-19 | AVO crossplots of intercept and gradient of S-2, R-2 and D-36  | 42 |
| Figure 3-20 | The workflow of pre-stack inversion  | 43 |
| Figure 3-21 | Statistical wavelet is extracted from full range of post-stack seismic and 180° phase rotation to match with data polarity using for seismic-well tie.                         | 44 |
| Figure 3-22 | CDP gathers and super gathers after muting   | 45 |
| Figure 3-23 | Super gathers overlying with incidence angle and angle gathers   | 45 |
| Figure 3-24 | The picking horizons on pre-stack seismic data   | 46 |
| Figure 3-25 | A series of wavelets extraction from well using for seismic inversion  | 46 |
| Figure 3-26 | Seismic to well correlation and cross-correlation using single wavelet   | 47 |
| Figure 3-27 | Cross section of P-impedance initial strata model  | 48 |

|             |   |    |
|-------------|---|----|
| Figure 3-28 | Example of pre-stack inversion analysis at D-36 well  | 48 |
| Figure 3-29 | Example results of the pre-stack inversion models along D-36 well A) Inverted $Z_P$ B) Inverted $Z_S$ C) Inverted $V_P/V_S$ and D) Inverted density   | 49 |
| Figure 4-1  | Results of the estimated $V_S$ and $V_P - V_S$ crossplot of D-36, $V_P$ log, existing $V_S$ log, estimated $V_S$ log  | 51 |
| Figure 4-2  | Synthetic seismogram and well to seismic correlation of S-2 well showing 75.5% of correlation coefficient after 17 ms of bulk shift   | 53 |
| Figure 4-3  | Synthetic seismogram and well to seismic correlation of R-2 well showing 53.4% of correlation coefficient after 13 ms of bulk shift   | 54 |
| Figure 4-4  | Synthetic seismogram and well to seismic correlation of D-36 well showing 65.4% of correlation coefficient after 14 ms of bulk shift  | 54 |
| Figure 4-5  | A series of wavelets extraction using wells for seismic inversion; Composite trace radius of angle gathers: 1, Angle range: 1 – 44 degree, Wavelet length: 120 ms and Time widow: horizon E to 500 ms below horizon O | 55 |
| Figure 4-6  | Amplitude spectrum extracting from seismic data represent the low frequency up to 12 Hz.  | 57 |
| Figure 4-7  | Seismic super gathers comparing to low pass frequency filter gathers, high pass frequency is 9 Hz and taper is 12 Hz that characteristic filter is (0, 0, 9, 12).   | 58 |
| Figure 4-8  | P-Impedance initial strata model and S-Impedance initial strata model using stacking velocity and well data   | 58 |
| Figure 4-9  | P-wave initial strata model and S-wave initial strata model using stacking velocity and well data   | 59 |
| Figure 4-10 | Density initial strata model and $V_P/V_S$ initial strata model using stacking velocity and well data   | 59 |



|             |   |    |
|-------------|---|----|
| Figure 4-11 | Crossplot between $\ln(Z_P)$ and $\ln(Z_S)$ and between $\ln(Z_P)$ and $\ln(D_n)$ , the both red lines can be moved for deriving the regression coefficients and the pre-whitening values.  | 61 |
| Figure 4-12 | Inversion analysis at D-36 well   | 62 |
| Figure 4-13 | Inversion analysis at R-2 well  | 62 |
| Figure 4-14 | Inversion analysis at S-2 well  | 63 |
| Figure 4-15 | Sections of inverted $Z_P$ , inverted $Z_S$ and inverted density along D-36 well overlying with their well logs   | 64 |
| Figure 4-16 | Sections of inverted $Z_P$ , inverted $Z_S$ and inverted density along S-2 well overlying with their well logs  | 65 |
| Figure 4-17 | Sections of inverted $Z_P$ , inverted $Z_S$ and inverted density along R-2 well overlying with their well logs  | 66 |
| Figure 4-18 | The horizon slices of horizon O (top Oligocene) extracting from inversion models of $Z_P$ , $Z_S$ , density and $V_P/V_S$   | 67 |
| Figure 4-19 | The horizon slices of horizon O (top Oligocene or FM0) extracting from inversion models of $Z_P$ , $Z_S$ , density and $V_P/V_S$ after changing color scale overlying by predicted channel sand trends of low $Z_P$ , $Z_S$ and density | 68 |
| Figure 4-20 | The horizon slices of horizon O+34ms extracting from inversion models of $Z_P$ , $Z_S$ , density and $V_P/V_S$ and changing color scale overlying by predicted channel sand trends of low $Z_P$ , $Z_S$ and density                     | 70 |
| Figure 4-21 | The horizon slices of horizon U (top FM1) extracting from inversion models of $Z_P$ , $Z_S$ , density and $V_P/V_S$ after changing color scale overlying by predicted channel sand trends of low $Z_P$ , $Z_S$ and density              | 71 |
| Figure 4-22 | The horizon slices of horizon C (top Unit 2C) extracting from inversion models of $Z_P$ , $Z_S$ , density and $V_P/V_S$ after changing color scale overlying by predicted channel sand trends of low $Z_P$ , $Z_S$ and density          | 72 |

- Figure 4-23 The horizon slices of horizon U-23ms extracting from inversion models of  $Z_P$ ,  $Z_S$ , density and  $V_P/V_S$  and changing color scale overlying by predicted channel sand trends of low  $Z_P$ ,  $Z_S$  and density 73
- Figure 5-1 Sections along B-35 well of inverted  $Z_P$  and inverted density overlying their well log 76
- Figure 5-2 Super gathers overlying with incidence angle and picking horizon show low angle of 21 degree at horizon O (the deepest horizon). 77



ลิขสิทธิ์มหาวิทยาลัยเชียงใหม่  
 Copyright© by Chiang Mai University  
 All rights reserved